# Reduced order modelling of an unstructured mesh air pollution model and application in 2D/3D urban street canyons

CrossMark

F. Fang [a, *], T. Zhang [b, a], D. Pavlidis [a], C.C. Pain [a], A.G. Buchan [a], I.M. Navon [c]

[a] Applied Modelling and Computation Group, Department of Earth Science and Engineering, Imperial College London, Prince Consort Road, London SW7 2BP, UK[1]
[b] State Key Laboratory of Hydraulic Engineering Simulation and Safety, Tianjin University, Tianjin 300072, China
[c] Department of Scientific Computing, Florida State University, Tallahassee, FL 32306-4120, USA

## HIGHLIGHTS

- A new POD reduced order model capable of resolving complex turbulent flows.
- POD combined with a LES adaptive mesh model based on an adapted Smagorinsky model.
- Efficient treatments of the nonlinear operators via the quadratic expansion method.
- Application to 2D/3D turbulent flows and pollution dispersion in urban landscapes.

## ARTICLE INFO

## ABSTRACT

A novel reduced order model (ROM) based on proper orthogonal decomposition (POD) has been developed for a finite-element (FE) adaptive mesh air pollution model. A quadratic expansion of the non-linear terms is employed to ensure the method remained efficient. This is the first time such an approach has been applied to air pollution LES turbulent simulation through three dimensional landscapes. The novelty of this work also includes POD's application within a FE-LES turbulence model that uses adaptive resolution. The accuracy of the reduced order model is assessed and validated for a range of 2D and 3D urban street canyon flow problems. By comparing the POD solutions against the fine detail solutions obtained from the full FE model it is shown that the accuracy is maintained, where fine details of the air flows are captured, whilst the computational requirements are reduced. In the examples presented below the size of the reduced order models is reduced by factors up to 2400 in comparison to the full FE model while the CPU time is reduced by up to 98% of that required by the full model.

© 2014 Published by Elsevier Ltd.

## 1. Introduction

Effective air quality management and response to air-quality emergencies necessitate the implementation of micro-scale models that are able to capture adequate spatial and temporal variability of urban emission dispersion. Recent work has revealed that the accuracy of simulated urban air flows and the dispersion of pollutants increases with the improved representation of the fluid's turbulent structures. However, current models available today are based on approaches that are either too computationally expensive to resolve within reasonable time scales, or fail to capture the detail of such complex problems. In this article a reduced order model is presented that aims to address this issue by presenting a method capable of resolving complex turbulent flows while avoiding the excessive computational requirements.

For general fluid flow problems, steady state Reynolds averaged numerical simulations (RANS) are now considered to be computationally inexpensive, however the approach can produce incorrect results, particularly when the flow is unsteady (Pope, 2000). Direct numerical simulations (DNS) on the other hand are capable of predictions that are indistinguishable from measurements (Coceal et al., 2007). DNS however has higher computational requirements that often impose restrictions on the size and complexity of the problems that can be solved. To model realistic urban flows, the best compromise between RANS and DNS is the large eddy simulation (LES) approach. This allows a better description of the turbulent structures without the excessive

* Corresponding author.
E-mail addresses: fangxinf@hotmail.com, f.fang@imperial.ac.uk (F. Fang).
[1] URL: http://amcg.ese.imperial.ac.uk.

computing costs. It can also be benefitted further, in terms of improved efficiency and accuracy, when developed within unstructured and adaptive frameworks that ensure resolution is placed to only the regions where it is required. However, even with these additional tools, complex 3D air flow problems may still require large computing resources; high fidelity solutions may therefore be unattainable for rapid response purposes.

For highly efficient simulations of flows, reduced order models (ROMs) present a powerful option of representing the dynamics of large-scale systems using only a smaller number of unknowns and reduced order basis functions. High-fidelity turbulence models can be projected onto reduced spaces, that are several orders of magnitude smaller than standard discrete models, so that their simulation can be computed efficiently. Not only does this enable the fast simulation of urban air flows, but also it allows a more interactive use of the model. Examples include applications of ROMs in the rapid determination of the impacts of pollutant sources (for emergency response), in ensemble calculations and in data assimilation.

Among existing reduced order methods, proper orthogonal decomposition (POD) has become popular due to its efficiency and accuracy in simulating fluid flows (Holmes et al., 2012). The technique entails determining the most energetic modes of a data set representing the flow, which are typically sets of snapshots taken at various time instances, and constructing optimal basis functions from them. However POD ROMs are normally constructed through a Galerkin projection, and this means they can suffer from numerical instabilities. In addition further adaptations are still required for the efficient treatment of the nonlinear terms within the partial differential equations (PDEs). Various ways for improving numerical stability to account for turbulence closure include the methods of subgrid-scale modelling, calibration, residual based stabilisation and Petrov–Galerkin POD (for details, see Bergmann et al., 2009; Fang et al., 2009a; Iollo et al., 2000; Galletti et al., 2004; Nguyen and Peraire, 2008; Balajewicz et al., 2013; Wang et al., 2012; Fang et al., 2013; Xiao et al., 2013). Successful non-linear treatments that remain efficient include the quadratic expansion method (Fang et al., 2009b; Du et al., 2013a), discrete empirical interpolation method (DEIM) (Nguyen and Peraire, 2008; Stefanescu and Navon, 2013), residual DEIM (RDEIM) (Xiao et al., 2014), and Gauss–Newton with approximated tensors (GNAT) (Carlberg et al., 2013). The successful application of POD spans across a wide range of fields. These include signal analysis and pattern recognition (Fukunaga, 1990), fluid dynamics and coherent structures (Holmes et al., 2012; Lumley, 1967; Aubry et al., 1988; Willcox and Peraire, 2002), image reconstruction (Kirby and Sirovich, 1990), ocean modelling (Cao et al., 2007; Fang et al., 2009b; Du et al., 2013a) and four-dimensional variational (4D-Var) data assimilation (Cao et al., 2007; Robert et al., 2005; Hoteit and Kohl, 2006; Daescu and Navon, 2008; Du et al., 2013b; Chen et al., 2011; Vermeulen and Heemink, 2006; Robert et al., 2006). More recently the POD approach has been incorporated within an unstructured mesh finite element ocean model (Fang et al., 2009a, 2009b; Du et al., 2013a), upon which the work within this article is based.

Recently, reduced order methods have been applied to air pollution (Sportisse and Djouad, 2000; Djouad and Sportisse, 2003; Debry and Sportisse, 2006; Sportisse and Djouad, 2007; Saunier et al., 2009; Bieringer et al., 2013; Alkuwari et al., 2013). Bieringer et al. (2013) utilised a multi-dimensional feature extraction and classification technique known as a self organizing map for reduction of the full climatological record into a subset of characteristic meteorological patterns and associated frequencies of occurrence. Alkuwari et al. (2013) used a new downscaling method based on fitted empirical orthogonal functions for an air quality model. Sportisse and Djouad (2007) introduced POD for reduction of chemical transport equations.

This article applies, for the first time, the POD–ROM approach to air pollution LES turbulent simulation. This new ROM is implemented within a novel LES adaptive mesh model, which is based on an adapted Smagorinsky model that uses the local flow length-scale to compute the sub-grid scale (SGS) viscosity. The use of the anisotropic Smagorinsky LES model introduces a diffusion term, thus improving the numerical stability. The model is applied to 2D/3D urban street canyon flows, and adaptive meshes are used to ensure all large energy-containing scales are resolved. Comparisons between the ROM and full model solutions are made to investigate the accuracy of the POD formulation. In this investigation a tracer puff release scenario is considered, and the tracer concentrations predicted by the model are compared at different space locations.

The remainder of this article is organized as follows. The full LES fluid model is described in Section 2. In Section 3 the details of the POD reduced order model are given. Section 4 presents 3 numerical examples of simulating urban air flows using the POD model. Conclusions are drawn in Section 5.

## 2. Governing equations

### 2.1. The 3D LES turbulent model

In LES, the larger scales of motions are numerically resolved while the effect of the smaller scales is modelled. This is accomplished by filtering the velocity field ($\widehat{\mathbf{u}}$) according to:

$$\mathbf{u}(\mathbf{x}, t) = \int_{\Omega} G(r, \mathbf{x})\widehat{\mathbf{u}}dr, \tag{1}$$

where $\Omega$ is the computational domain, $\mathbf{x}$ are the Cartesian coordinates, $r$ the radial coordinates and G represents the filter. The filter has the effect of removing those scales of motion smaller than the filter width $F$. The specified filter function G satisfies the normalisation condition:

$$\int_{\Omega} G(r, \mathbf{x})dr = 1. \tag{2}$$

The underlying model equations used here consist of the continuity equation and incompressible Navier–Stokes equations of the filtered quantities. Assuming an eddy viscosity approach, the equations are given as:

$$\nabla \cdot \mathbf{u} = 0, \tag{3}$$

$$\frac{\partial \mathbf{u}}{\partial t} + \mathbf{u} \cdot \nabla \mathbf{u} = -\nabla p + \nabla \cdot \boldsymbol{\tau}, \tag{4}$$

where $\mathbf{u} \equiv (u,v,w)^T \equiv (u_1,u_2,u_3)^T$ is the velocity vector, $p$ is the modified pressure, and $\boldsymbol{\tau}$ is the viscous stress term.

The viscous stress term is:

$$\boldsymbol{\tau} = \left(\nu_f + \nu_\tau\right) \cdot \nabla \boldsymbol{u}, \tag{5}$$

where $\nu_f$ is the kinematic viscosity and $\nu_\tau$ is the LES sub-grid scale viscosity which is calculated using an anisotropic Smagorinsky model (Aristodemou et al., 2009). The advantage of the anisotropic Smagorinsky model used here over existing Smagorinsky models is that it combines the LES model with a fully adaptive unstructured mesh, in order to optimize resolution throughout the flow. Such a

combination allows us to capture and analyse the complex flow features expected at street canyons and intersections in detail, whilst making best use of the computational resources. In our anisotropic mesh adaptive simulations the length scale is related directly to the local flow length scale and varies with space, time and coordinate direction. More information can be found in one of our previous publications that discusses LES modelling (see Aristodemou et al., 2009).

In the filtered Navier–Stokes equations, the sub-grid scale (SGS) tensor term from equation (4) is modelled as:

$$\frac{\partial \tau_{ij}}{\partial x_j} = \frac{\partial}{\partial x_i}\left[\nu_{jk}\frac{\partial u_j}{\partial x_k}\right],\tag{6}$$

where $\nu_{jk}$ is a tensorial eddy-viscosity.

The local length-scale of the flow in each direction is already calculated as part of the mesh adaptivity technology embedded in the *Fluidity* model (Pain et al., 2001). This fact has been used to develop a novel tensorial model for the eddy viscosity. The tensorial eddy viscosity can be written as:

$$\nu_\tau = \begin{bmatrix} \nu_{xx} & \nu_{xy} & \nu_{xz} \\ \nu_{yx} & \nu_{yy} & \nu_{yz} \\ \nu_{zx} & \nu_{zy} & \nu_{zz} \end{bmatrix} = R^T \begin{bmatrix} \nu_{\zeta\zeta} & 0 & 0 \\ 0 & \nu_{\eta\eta} & 0 \\ 0 & 0 & \nu_{\xi\xi} \end{bmatrix} R,\tag{7}$$

where the multiplication by $R^T$ and $R$ represents the rotation from the local coordinate system $(\zeta,\eta,\xi)$ to the global simulation coordinate system. Employing the Smagorinsky model in each direction:

$$\nu_\tau = C_S^2\left|\tilde{S}\right| R^T \begin{bmatrix} \Delta_\zeta^2 & 0 & 0 \\ 0 & \Delta_\eta^2 & 0 \\ 0 & 0 & \Delta_\xi^2 \end{bmatrix} R,\tag{8}$$

where $C_S$ is the Smagorinsky coefficient ($C_S$ = 0.1) and $\left|\tilde{S}\right| = (2S_{ij}S_{ij})^{1/2}$, where $S_{ij} = 1/2((\partial u_i/\partial x_j) + (\partial u_j/\partial x_i))$ is the rate of strain tensor.

The filter width for separation into resolved and unresolved scales is set to twice the local element size ($h_\zeta,h_\eta,h_\xi$). This allows a truer representation of the resolved scales than the conventional approach of setting the filter equal to the element size (Pope, 2000):

$$\nu_\tau = 4C_S^2\left|\tilde{S}\right| R^T \begin{bmatrix} h_\zeta^2 & 0 & 0 \\ 0 & h_\eta^2 & 0 \\ 0 & 0 & h_\xi^2 \end{bmatrix} R.\tag{9}$$

In the second-order SGS model the viscous or diffusion operator is evaluated at each quadrature point with the usual finite element treatment of the second-order terms. That is by applying Green's theorem to the weighted residual equations using a Bubnov–Galerkin method.

### 2.2. Pollutant transport modelling

The dispersion of the tracer concentration ($c$) is modelled by:

$$\frac{\partial c}{\partial t} + \mathbf{u}\cdot\nabla c + \nabla\cdot(\kappa\nabla c) - Q = 0,\tag{10}$$

where $Q$ is a source term and $\kappa$ the diffusivity.

This transport equation is solved over control volumes (CV) through the use of function $M_{CV}$ which is unity over CV and zero otherwise:

$$\int_\Omega M_{CV_i}\left(\frac{\partial c}{\partial t} + \mathbf{u}\cdot\nabla c + \nabla\cdot(\kappa\nabla c) - Q\right)d\Omega = 0.\tag{11}$$

## 3. A POD reduced order air pollution model

### 3.1. Proper orthogonal decomposition

Let the model variable solutions $\{V_k(\mathbf{x},t_k)\}$ (*e.g.* either one of the velocity components $u,v,w$ or pressure $p$) form a set of snapshots sampled at the defined checkpoints during the simulation $[t_1,\ldots,t_k,\ldots,t_K]$, where $K$ is the number of snapshots. The average of the ensemble of snapshots is defined as:

$$\overline{V} = \frac{1}{K}\sum_{k=1}^{K}V_k,\tag{12}$$

and the deviation from the mean of variables is defined as:

$$\tilde{V}_k = V_k - \overline{V}.\tag{13}$$

The goal of POD is to find a set of orthogonal basis functions $\{\Phi_k\}$ such that it maximises

$$\frac{1}{K}\sum_{k=1}^{K}\left|<\tilde{V}_k,\Phi_k>_{L^2}\right|^2,\tag{14}$$

subject to

$$\sum_{k=1}^{K}|<\Phi_k,\Phi_k>_{L^2}|^2 = 1,\tag{15}$$

where $<\cdot,\cdot>_{L^2}$ is the canonical inner product in $L^2$ norm. The approach introduced by Sirovich (1987) is used to find an optimal set of basis functions $\Phi$ of the optimisation problem (14). The POD bases can be written as a linear combinations of the snapshots $\tilde{V}_k$:

$$\Phi_k = \sum_{k=1}^{K}y_k\tilde{V}_k; \quad 1 \leq k \leq K,\tag{16}$$

where $y_k$ are the eigenvectors which can be obtained by solving a $K \times K$ eigenvalue problem below:

$$\mathscr{C}y_k = \lambda_k y_k; \quad 1 \leq k \leq K,\tag{17}$$

where $\mathscr{C}$ is the $K \times K$ matrix with $\mathscr{C}_{k,l} = (1/K)<\tilde{V}_k,\tilde{V}_l>$ $(1 \leq k,l \leq K)$. The eigenvalues $\lambda_k$ are real and positive and should be ordered in descending order. The $k^{th}$ orthogonal eigenvalue $y_k$ is a measure of the kinetic energy contained within the $k^{th}$ basis.

In this work, the POD basis vectors for $u,v,w$ and $p$ are calculated from the snapshots of the solutions for each variable $u,v,w$ and $p$ respectively. Different POD numbers can be chosen for different variables. The key issue consists in forming an effective reduced order model so as to obtain a set of snapshots which should include as much as information for generating the POD basis functions. More POD snapshots as well as more POD bases should be retained for a realistic representation of flow dynamics on a wide range of

scales. An increase in the number of snapshots and POD bases leads to an improvement in the accuracy of the POD model.

### 3.2. Implementation of a POD air pollution model

In POD, any variable $V(t,x,y,z)$ (here, $u,v,w,p$) can be expressed as an expansion of the POD basis functions:

$$V(t,x,y,z) = \overline{V} + \sum_{m=1}^{M} \alpha_{m,V}(t)\Phi_{m,V}(x,y,z), \tag{18}$$

where $\Phi_{m,V}(x,y,z)$ is the POD basis functions for $V$, $\alpha_{m,V}(t)$ is the corresponding coefficient, $1 \leq m \leq M$ and $M$ is the number of the POD basis functions. For simplicity, equations (3), (4) and (10) can be re-written in a general form:

$$\frac{\partial V}{\partial t} = F(V). \tag{19}$$

Taking the POD basis function as the test function, then integrating (19) over the computational domain $\Omega$, yields:

$$\left\langle \frac{\partial V}{\partial t}, \Phi_{m,V} \right\rangle_{\Omega} = \langle F(V), \Phi_{m,V} \rangle_{\Omega}. \tag{20}$$

Substituting (18) into (20), the POD reduced order equations are then obtained:

$$\frac{\partial \alpha_{m,V}}{\partial t} = \left\langle F\left(\overline{V} + \sum_{m=1}^{M} \alpha_{m,V}(t)\Phi_{m,V}(\mathbf{x})\right), \Phi_{m,V} \right\rangle_{\Omega}, \tag{21}$$

subject to the initial condition

$$\alpha_{m,V}(0) = \left( (V(0,\mathbf{x}) - \overline{V}(\mathbf{x})), \Phi_{m,V} \right). \tag{22}$$

The POD ROM (21) has been implemented using the approach proposed in Du et al. (2013a), that is, by projecting the matrix and source term vector of the full discrete model onto the reduced space. The implementation of reduced order modelling codes involves only the matrix vector multiplication of the full model. Importantly, the code is largely independent of the implementation details of the original equations. For nonlinear problems, a perturbation approach is used to help accelerate the matrix equation assembly process, based on the assumption that the discretized system of equations has a polynomial representation and can thus be created by a summation of pre-formed matrices. For more details see Fang et al. (2009b), Du et al. (2013a). The errors for the above POD model are bounded by the following expression (details of the derivation can be found in Fang et al. (2009b)):

$$\left\| V_{\text{full}} - V \right\|_2 \leq \sqrt{\lambda_{(M+1)}}, \tag{23}$$

where $V_{\text{full}}$ is the reference solution calculated by the full model, and $\lambda_{M+1}$ is the $(M+1)^{\text{th}}$ eigenvalue (*i.e.* the largest singular eigenvalue truncated by the POD approach) for variable $V$.

## 4. Tracer dispersion in an urban street canyon

The POD reduced order air pollution model has been developed with a 3D unstructured and adaptive mesh model, which is capable of simulating flows on a wide range of horizontal and vertical scales (Pain et al., 2005). The model employs 3D anisotropic mesh adaptivity to resolve fine scale features as they develop while reducing resolution elsewhere. The mesh adaptivity is guided by a-priori absolute interpolation error of the velocity field (for further details,

see Pain et al., 2001). The transition from the finer regions to the coarser ones is smooth through the use of an anisotropic linear gradation parameter in the mesh adaptivity algorithm (Pain et al., 2001). This ensures that adjacent element edge length differences do not exceed 30%. A simple point-wise interpolation method is used for mesh-to-mesh interpolations between adaptations. This method is bounded but it is non-conservative and it is also diffusive. More sophisticated (conservative) methods are available but are omitted at this stage to keep computations simple. The anisotropic Smagorinsky LES model is used for improving the stability of the Galerkin POD–ROM.

As already discussed, the reduced order model is formed by projecting the original model from a high dimensional space onto a reduced space. A set of optimal basis functions are obtained from pre-computed solutions sampled at pre-specified time instances (referred to as snapshots). The quality of the resultant reduced order model depends highly on the choice of snapshots. Adaptive mesh refinement is an efficient way to reduce computational complexity and to provide high resolution snapshots for the reduced order model.

The accuracy of the new POD reduced order air pollution model is assessed and validated in three cases: 2D and 3D street canyon flows as well as the tracer study of dispersion in a 2D canyon street. These test cases are dimensionless. A comparison between the results obtained with the full and reduced order models has been carried out.

### 4.1. Case1: 2D street canyon flows

The model has been used to simulate flow past an infinite series of 2D street canyons which have unity height-to-width aspect ratio. The geometry and mesh (consisting of 17,228 nodes and 33,588 elements) used for this simulation is shown in Fig. 1. The boundary layer depth is five times the building height. At least 60 surface elements cover each building surface. The mesh is uniform within the canyon and the elements gradually increase in size with height. The inflow boundary condition is periodic, which ensures a fully developed boundary layer. The kinematic viscosity is set to $1 \times 10^{-4}$. The Reynolds number, based on the building height and the maximum velocity, is $10^4$. No-slip boundary conditions are applied on the domain's bottom edge and all building surfaces. A free-slip boundary condition is applied on the domain's top boundary. The flow is driven by a prescribed pressure gradient across the domain, and this results in an approximate maximum velocity of 1. The time step size is set to 0.01 which ensures the
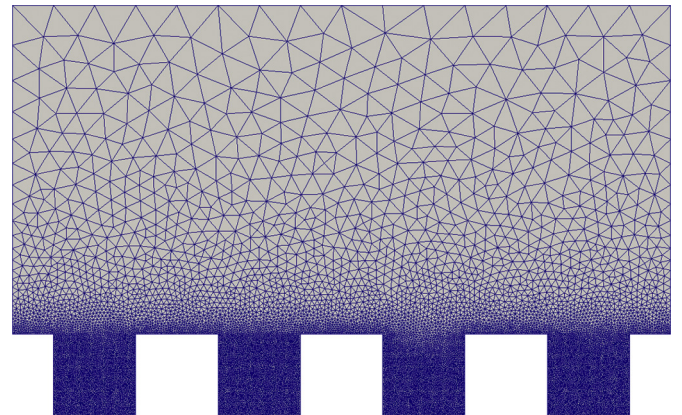


**Fig. 1.** Case 1: Computational domain and unstructured mesh.

(a) $t = 3$ (left: full model; right: reduced order model)



(b) $t = 4$ (left: full model; right: reduced order model)
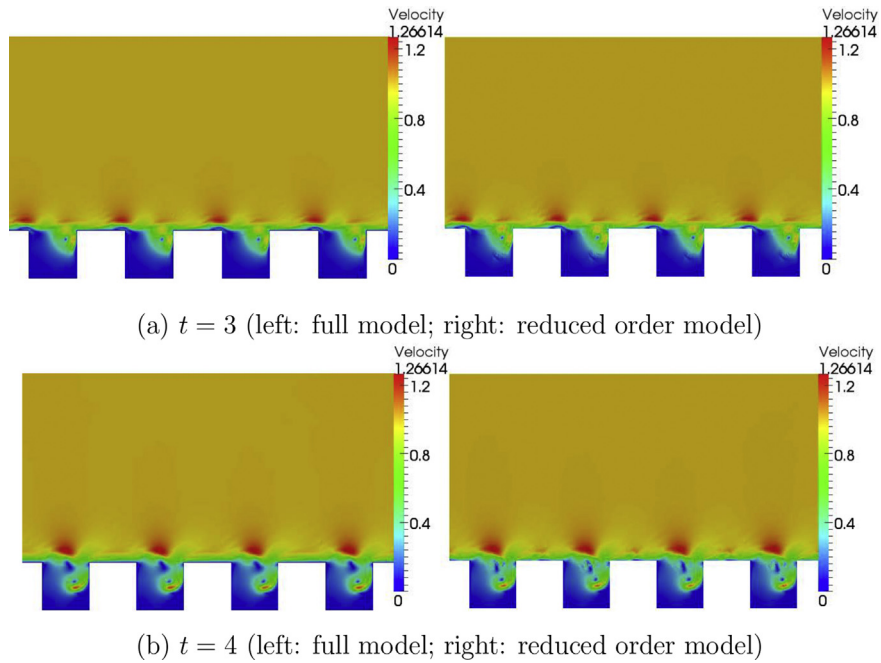
**Fig. 2.** Case 1: velocity results obtained from the full (left panel) and reduced order (right panel) models.

Courant–Friedrichs–Lewy (CFL) number, defined as $\Delta t \mathbf{J}^{-1} \mathbf{u}$ (where $\mathbf{J}$ is the finite element Jacobian matrix), remains under 0.99 for numerical stability purposes.

Fifty snapshots were taken from the pre-computed solution at every fourth time level and from these 40 basis functions were generated for $u$, $v$, $w$ and $p$. These basis functions captured 99% of 'energy'. With the original FE model consisting of 17,228 nodes, the problem size is reduced by a factor of 430. The accuracy of the POD ROM is evaluated by comparing its solution with that of the full model, and these are shown in Fig. 2. It is shown that both model solutions are in good agreement with each other and that the

structures of the eddies inside the canyons are captured. Fig. 3 presents the absolute errors of the ROM at the time instances 3 and 4. Whilst the largest errors do occur around the top section of the canyons they mainly remain below 0.06. Larger errors at the time instance $t = 4$ do occur but these remain restricted to very small regions.

### 4.2. Case 2: 3D street canyon flows

To demonstrate the ROM's ability to simulate 3D flows, the model is applied to resolving flow past two buildings. The domain



(a) $t = 3$

(b) $t = 4$
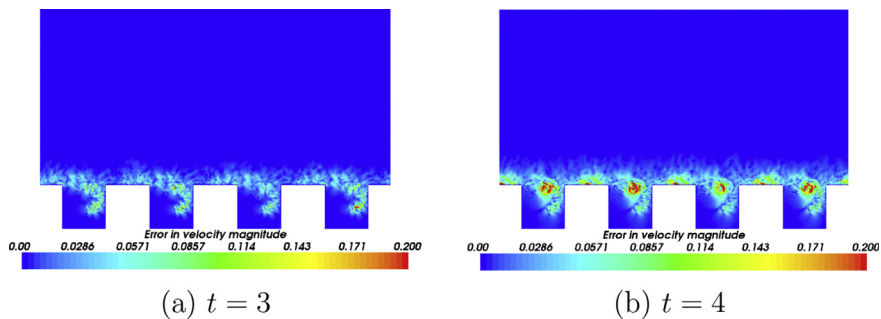
**Fig. 3.** Case 1: Error in the velocity solution obtained from the reduced order model as compared with the high fidelity model.
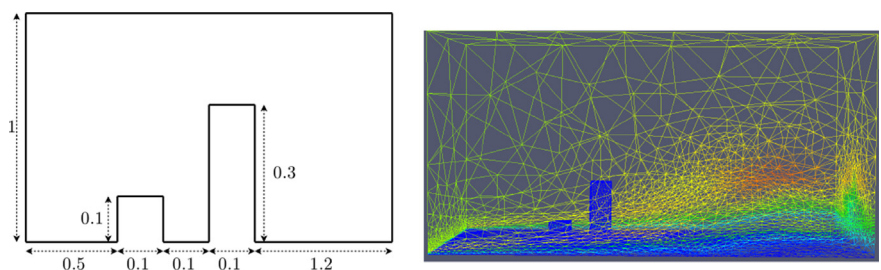


**Fig. 4.** Case 2: Computational domain, unstructured mesh and a 2D schematic of the building with a width of 0.1.

(a) $t = 2.4$                                                                        (b) $t = 3.1$
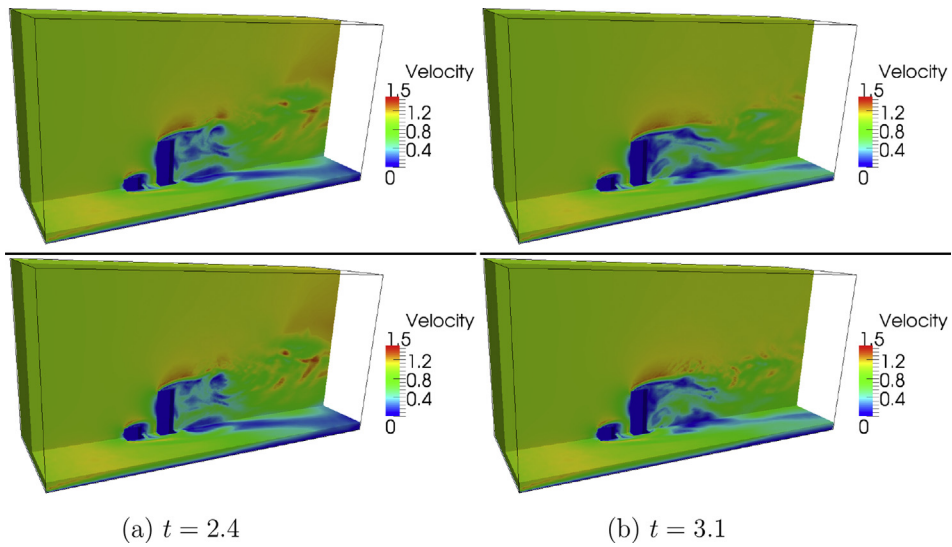
**Fig. 5.** Case 2: velocity results (in both the horizontal and vertical cross sections) obtained from the full (top panel) and reduced order (bottom panel) models.

and mesh are shown in Fig. 4 which includes a 2D schematic of the building's height and positions. The size of the domain is 2 × 0.7 in the horizontal and 1 in the vertical. The buildings are located on the domain centreline.

A uniform velocity of 1 is prescribed on the inflow boundary located on the domain's left side. No-slip boundary conditions are applied on the domain's bottom edge and all building surfaces. A free-slip boundary condition is applied on the domain's top
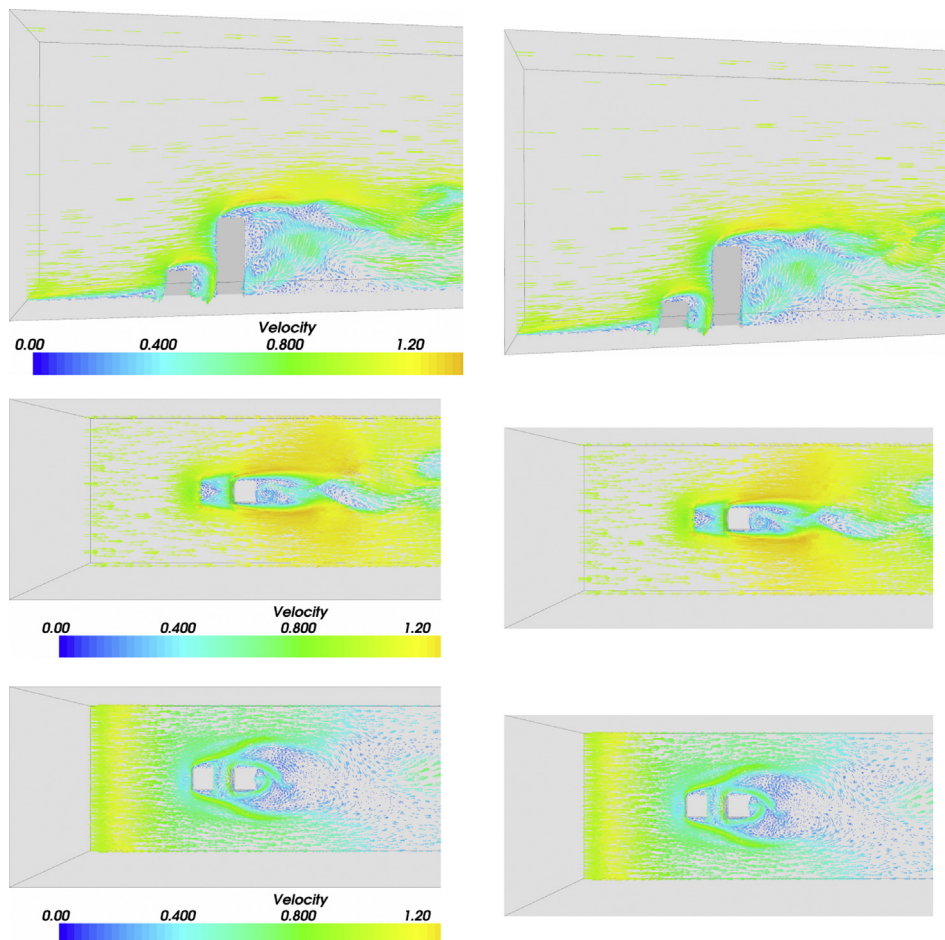


**Fig. 6.** Case 2: Velocity vector field at different cross section at time level $t = 3.1$. Left: full model and right: reduced order model (top panel: vertical cross section at the centreline of the buildings; middle panel: the horizontal cross section at $z = 0.1$; bottom panel: the horizontal cross section at $z = 0.3$).
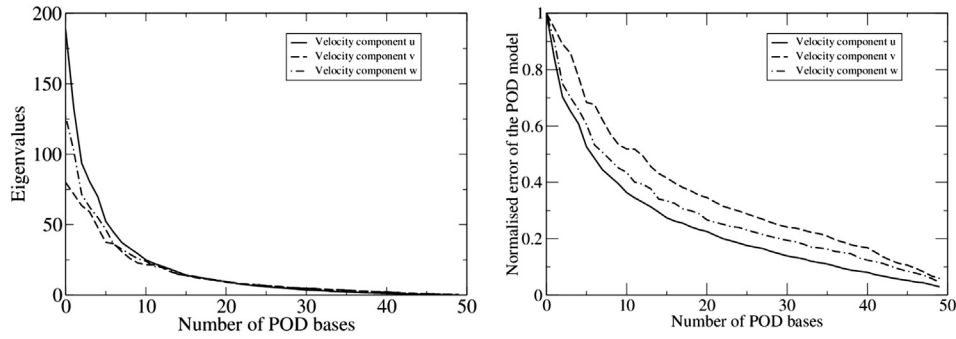
**Fig. 7.** Case 2: Eigenvalues and normalised errors for velocity components $u$, $v$ and $w$ (left panel: eigenvalues; right panel: normalised error of the POD model). The errors for the POD model are bounded by equation (23), that is, the squared root of the $(M+1)^{th}$ eigenvalue (the largest neglected singular eigenvalue). $M$ is the number of eigenvectors (POD bases) chosen for each variable. The error decreases as the number of POD bases chosen is increased.

boundary. The kinematic viscosity is set to $1 \times 10^{-5}$. The Reynolds number is $2 \times 10^4$ based on the average building height and the reference velocity of 1. The time step size is set to 0.008 which ensures the CFL number remains under 0.99.

Adaptive mesh refinement of the full FE model is used in this simulation for building the ROM model. Starting with a uniform coarse mesh the full model adapts every 20 time steps with the maximum and minimum element size of 0.5 and 0.01 respectively. A relatively fine mesh consisting of 96,667 nodes and 539,364

elements is achieved when $t = 1.592$. From this point in time the fine mesh is fixed and the FE model continues to simulate the flow over the time period [1.592, 3.192]. During this period snapshots are recorded with all having the same length of 96,667. In total 50 snapshots are taken at every fourth time level (here, each time level is set to 0.01), and from these 40 POD basis functions are generated for $u$, $v$, $w$ and $p$ (for which 99% of 'energy' is captured). Comparing with the size of the original FE model the resulting ROM's size is smaller by a factor of 2400.



(a) $t = 2.4$ (50 snapshots with 40 POD bases)  (b) $t = 3.1$ (50 snapshots with 40 POD bases)

(c) $t = 3.1$ (50 snapshots with 12 POD bases)  (d) $t = 3.1$ (12 snapshots with 12 POD bases)
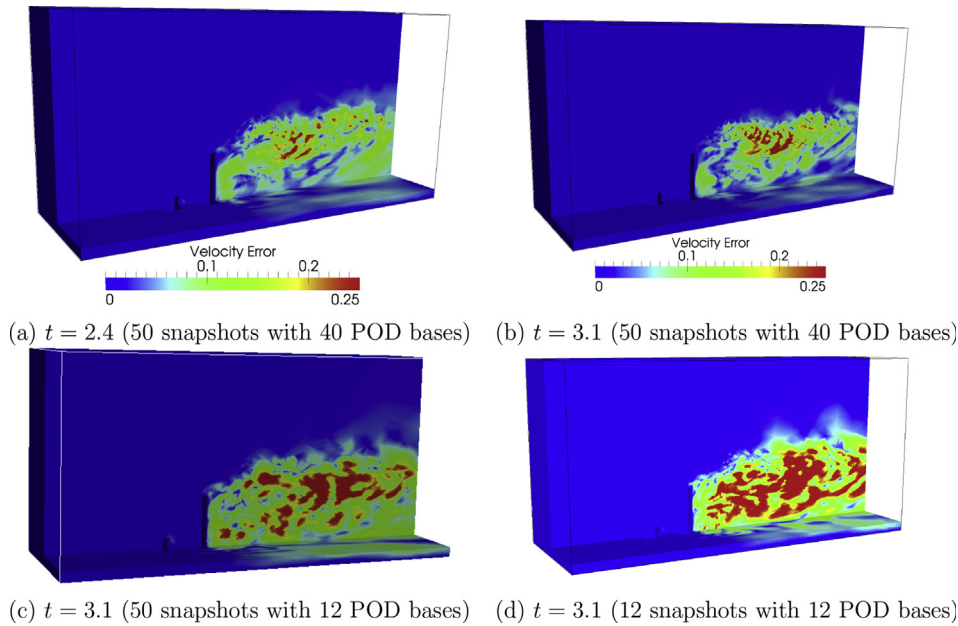
**Fig. 8.** Case 2: Absolute error in the POD velocity solution at time levels $t = 2.4$ and 3.1 (in both the horizontal and vertical cross sections). The POD ROM is constructed with the use of 50 snapshots and (a)–(b) 40 POD bases; (c) 12 POD bases; as well as (d) 12 snapshots with 12 POD bases.
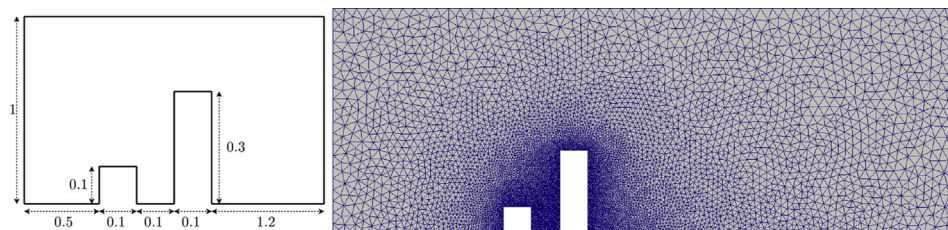


**Fig. 9.** Case 3: Computational domain and unstructured mesh.
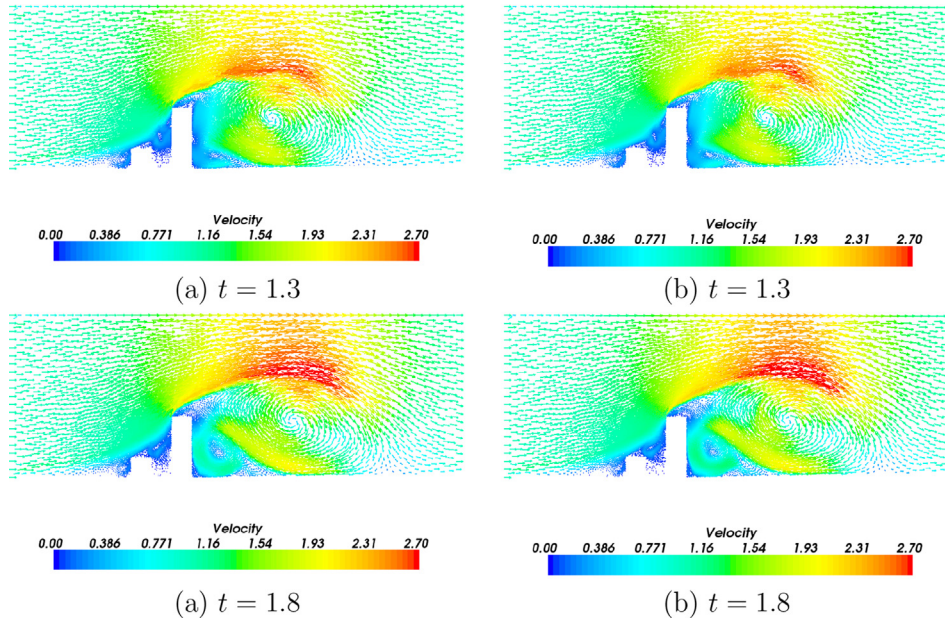
Fig. 10. Case 3: Velocity vector field obtained from the full (left panel) and reduced order (right panel) models.
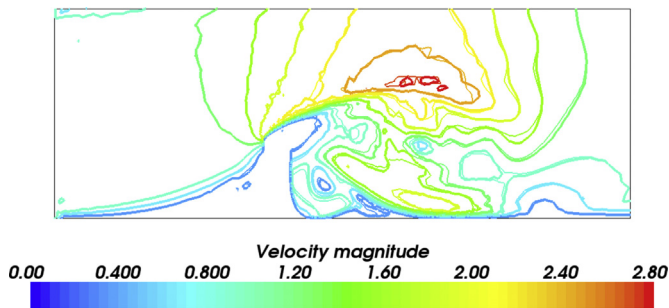


Fig. 11. Case 3: Comparison of velocity contours obtained from the full (thick line) and reduced order (thin line) models at time level $t = 1.8$.

The solutions at times $t = 2.4$ and $t = 3.1$ from both the POD and full model are presented in Figs. 5 and 6. The velocities in both the horizontal and vertical cross sections are overall in good agreement with each other. POD is shown to have performed well at capturing the complex flow patterns around the buildings.

To further address the quality of the POD ROM, the corresponding error estimation of the POD ROM has been carried out in this work. The errors in the ROM solutions are shown in Fig. 8. It can be seen that the error in the POD solutions can be reduced by increasing the number of the snapshots and POD bases. There is a trade-off between the accuracy and the CPU time. In this work, 50 snapshots are chosen so that the error of the POD results remains relatively small (less than 0.25) in large regions of the domain,
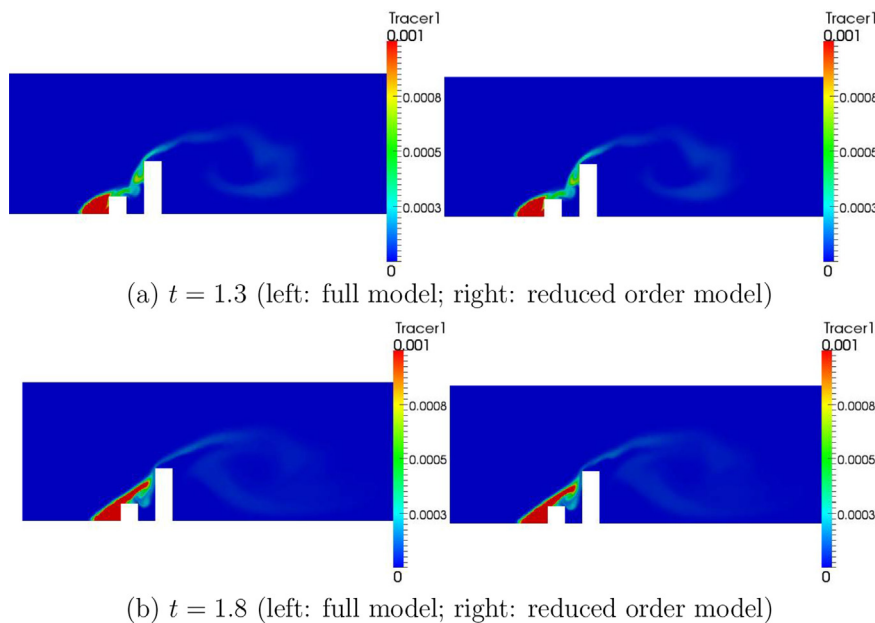


Fig. 12. Case 3: Tracer 1 concentration obtained from the full (left panel) and reduced order (right panel) models, where the magnitude of the concentration is capped.

(a) $t = 1.3$ (left: full model; right: reduced order model)



(b) $t = 1.8$ (left: full model; right: reduced order model)
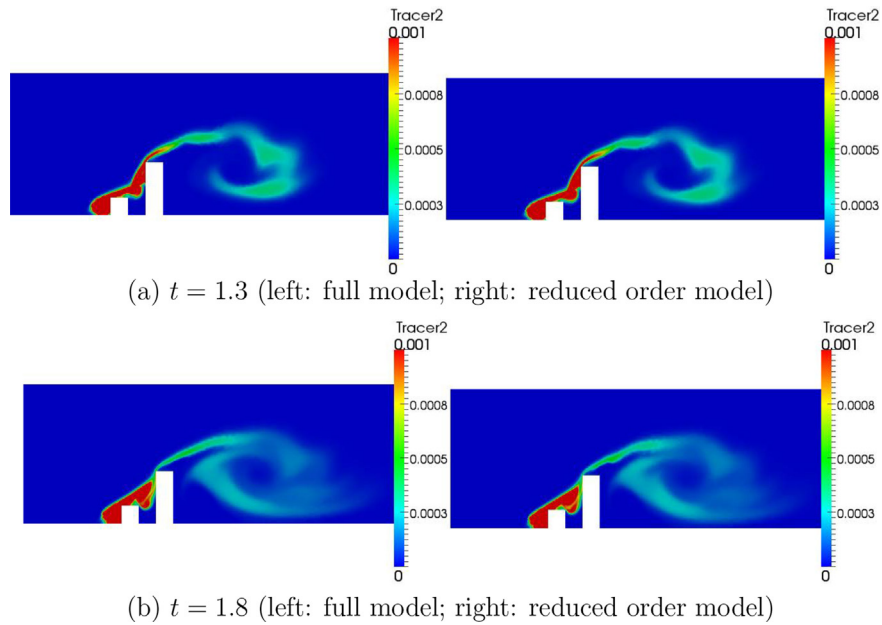
**Fig. 13.** Case 3: Tracer 2 concentration obtained from the full (left panel) and reduced order (right panel) models, where the magnitude of the concentration is capped.

therefore the POD results are considered to be closer to those obtained from the full model.

Fig. 7 presents the eigenvalues and the normalised errors in velocity results obtained from the POD model (calculated by equation (23)) for a given number of POD basis functions for each of the velocity components $u$, $v$ and $w$. The first graph displaying the eigenvalues shows a steep decline in the energy lost as the number of POD functions is increased. Accordingly, the graph presenting the predicted errors in velocity results shows that there is a sharp decrease in the error size as the number of POD functions is increased. Using 20 POD functions the error decreases by approximately 60% in comparison to using just one POD function. Using 40 functions this error decreases sufficiently to a predicted 2-norm value of 0.15.

### 4.3. Case 3: dispersion of tracers in a 2D street canyon

In this final example the ROM model is applied to the simulation of the dispersion of three polluting sources within a 2D urban landscape. The geometry of the problem is rectangular in shape, with a length of 2 and a height of 1, and contains two neighbouring buildings that form a canyon between them. The geometry of the problem is presented in Fig. 9. The figure also displays the unstructured mesh used in the full FE model. This mesh remains fixed in the full simulation and consists of 8264 nodes and 33,588 elements. The three polluting tracer sources (within a radius of 0.005) are positioned against the left face of the smaller building, and in turn are placed at heights 0.025, 0.05 and 0.1, respectively. These are continuous sources that are released into the domain at a rate of 1.



(a) $t = 1.3$ (left: full model; right: reduced order model)



(b) $t = 1.8$ (left: full model; right: reduced order model)
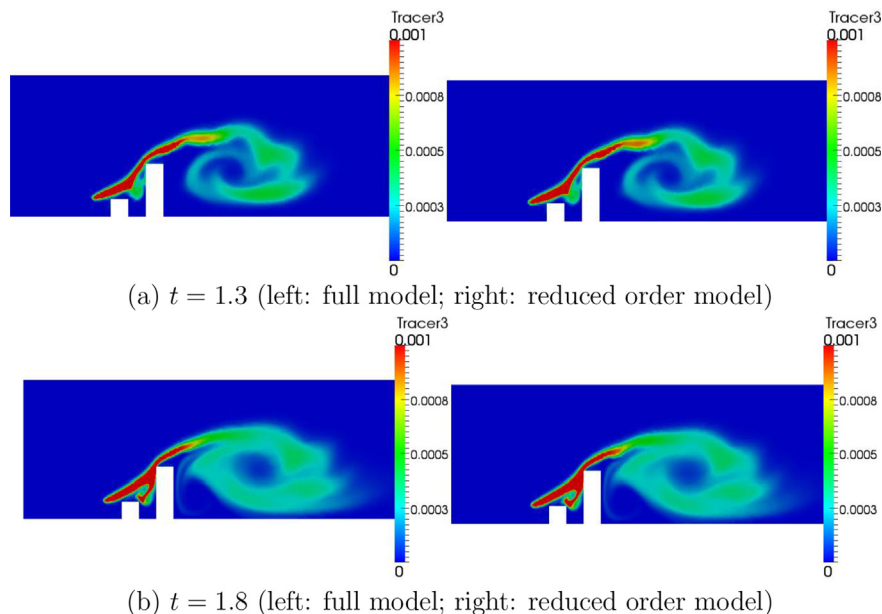
**Fig. 14.** Case 3: Tracer 3 concentration obtained from the full (left panel) and reduced order (right panel) models, where the magnitude of the concentration is capped.

(a) $t = 1.3$

(b) $t = 1.8$
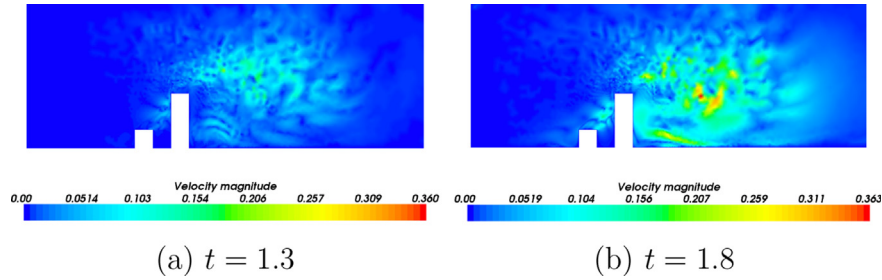
**Fig. 15.** Case 3: Absolute error in the velocity results obtained from the reduced order model.

A uniform velocity of 1 is prescribed on the inflow boundary located on the left side of the domain. No-slip boundary conditions are applied on the domain's bottom edge and all building surfaces. A free-slip condition is applied on the domain's top boundary. The kinematic viscosity is set to $1 \times 10^{-4}$ and the Reynolds number equates to $1 \times 10^4$. A zero boundary condition is imposed at the inflow positions of all tracers.

The full simulation was allowed to run to $t = 0.79$, which was sufficient time to allow the eddies to form. Following this the full simulation was run to $t = 1.8$ using a time step of 0.008. Over this time period [0.79, 1.8] the solutions were recorded at every tenth time step (every 0.08), resulting in a total of 50 snapshots. From these snapshots 40 POD basis functions were constructed for each of the solution variables, and these bases were capable of capturing 99% of their energy whilst reducing the size of the problem by a factor of 200.

Fig. 10 presents the velocity vector field solutions predicted by the full and POD models at two time instances. The two sets of results are in close agreement and show the ROM model to have captured well the eddies forming through the domain. Fig. 11 presents the velocity contours from both models at time $t = 1.8$. Again there is close agreement between the models where even the small features in the velocities are captured by the ROM.

The three tracer concentration solutions predicted by the full and reduced order models are presented in Figs. 12–14. These solutions are shown at time instances $t = 1.3$, 1.8 and once again good agreement is observed between the two models. In particular the ROM has performed very well at resolving the concentration of tracer 3 where beyond the second building it forms a complex flow pattern.

The errors in the ROM's velocity and tracer solutions at times 1.3 and 1.8 are presented in Figs. 15 and 16 respectively. In general the errors in the velocities are relatively small, typically less than 0.15, however there are locally larger errors that have formed but these are restricted to small regions of the domain. The tracer errors are shown to be very low in value and rarely exceed 0.0001 for all concentrations.

Table 1 shows the CPU time of main process at each time step. It can be seen that the reduced order model saves 78–98% of CPU time required by the full model.

## 5. Conclusions

This article has presented the first reduced order model for use in simulating air and pollution flow through urban streets and



(a) Tracer 1: $t = 1.3$

(b) Tracer 1: $t = 1.8$

(a) Tracer 2: $t = 1.3$

(b) Tracer 2: $t = 1.8$

(a) Tracer 3: $t = 1.3$

(b) Tracer 3: $t = 1.8$
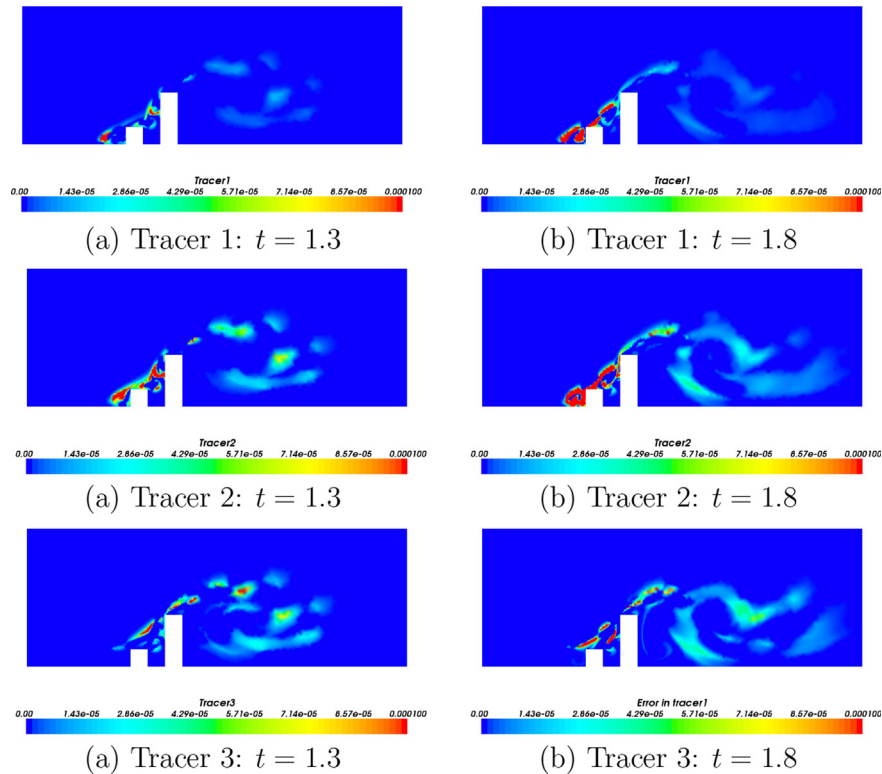
**Fig. 16.** Case 3: Absolute error in the tracer concentrations obtained from the reduced order model.

**Table 1**
Comparison of CPU (unit: s) required for running the full model and ROM for each time step.

|  |  | Assembling matrices | Solving | Total |
|---|---|---|---|---|
| Case1 (2D) | Full model | 1.62 | 1.24 | 2.86 |
|  | POD ROM | 0.64 | 0.04 | 0.68 |
| Case2 (3D) | Full model | 53.62 | 14.54 | 68.16 |
|  | POD ROM | 1.4 | 0.06 | 1.46 |
| Case3 (2D) | Full model | 1.62 | 3.34 | 4.96 |
|  | POD ROM | 0.64 | 0.74 | 1.38 |

landscapes using a FE-LES turbulent model with adaptive resolution meshes. In this formulation POD was used to construct optimal basis functions from solution snapshots produced by the full LES model, and the ROM then formed through a Galerkin projection over this basis set. A quadratic expansion of the non-linear terms was employed to ensure the method remained efficient and thus avoid employing POD–DEIM.

The reduced order model has been applied to three test cases involving air and pollution flow through urban landscapes. Both two and three dimensional problems of varying difficulty have been used, and comparisons between the ROM and full model solutions were made to determine the accuracy of the proposed method. In all cases the ROM was shown to accurately capture the flow details as both its velocity and tracer profiles showed good agreement with the full FE model. Without compromising the solution's accuracy the ROM model was able to reduce the problem size by several orders of magnitude. In comparison to the full model the problem sizes were reduced by factors of 200–2400, while the CPU time was correspondingly reduced 78%–98% of that required by the full model in the examples presented.

## Acknowledgements

## References

Alkuwari, F.A., Guillas, S., Wang, Y., 2013. Statistical downscaling of an air quality model using fitted empirical orthogonal functions. Atmos. Environ. http://dx.doi.org/10.1016/j.atmosenv.2013.08.031.

Aristodemou, E., Bentham, T., Pain, C., Colvile, R., Robins, A., ApSimon, H., 2009. A comparison of mesh-adaptive LES with wind tunnel data for flow past buildings: mean flows and velocity fluctuations. Atmos. Environ. 43, 6238–6253.

Aubry, N., Holmes, P., Lumley, J.L., 1988. The dynamics of coherent structures in the wall region of a turbulent boundary layer. J. Fluid Dyn. 192, 115–173.

Balajewicz, M.J., Dowell, H.E., Noack, B.R., 2013. Low-dimensional modelling of high-Reynolds-number shear flows incorporating constraints from the Navier-Stokes equation. J. Fluid Mech. 729, 285–308.

Bergmann, M., Bruneau, C.H., Iollo, A., 2009. Enablers for robust POD models. J. Comput. Phys. 228 (2), 516–538.

Bieringer, P.E., Longmore, S., Bieberbach, G., Rodriguez, L.M., Copeland, J., Hannan, J., 2013. A method for targeting air samplers for facility monitoring in an urban environment. Atmos. Environ. 80, 1–12.

Cao, Y., Zhu, J., Navon, I.M., Luo, Z., 2007. A reduced order approach to four-dimensional variational data assimilation using proper orthogonal decomposition. Int. J. Numer. Methods Fluids 53 (10), 1571–1583.

Carlberg, K., Farhat, C., Cortial, J., Amsallam, D., 2013. The GNAT method for nonlinear model reduction: effective implementation and application to computational fluid dynamics and turbulent flows. J. Comput. Phys. 242, 623647.

Chen, X., Navon, I.M., Fang, F., 2011. A dual weighted trust-region adaptive POD 4D-Var applied to a finite-element shallow water equations model. Int. J. Numer. Methods Fluids 65 (5), 520–541.

Coceal, O., Dobre, A., Thomas, T.G., Belcher, S.E., 2007. Structure of turbulent flow over regular arrays of cubical roughness. J. Fluid Mech. 589, 375–409.

Daescu, D.N., Navon, I.M., 2008. A dual-weighted approach to order reduction in 4D-Var data assimilation. Mon. Weather Rev. 136 (3), 1026–1041.

Debry, E., Sportisse, B., 2006. Reduction of the condensation/evaporation dynamics for atmospheric aerosols: theoretical and numerical investigation of hybrid methods. J. Aerosol Sci. 37 (8), 950–966.

Djouad, R., Sportisse, B., 2003. Solving reduced chemical models in air pollution modelling. Appl. Numer. Math. 44 (12), 49–61.

Du, J., Fang, F., Pain, C.C., Navon, I.M., Zhu, J., Ham, D., 2013. POD reduced-order unstructured mesh modelling applied to 2D and 3D fluid flow. Comput. Math. Appl. 65, 362–379.

Du, J., Navon, I.M., Zhu, J., Fang, F., Alekseev, A.K., 2013. Reduced order modeling based on POD of a parabolized Navier-Stokes equations model II: trust region POD 4-D VAR data assimilation. Comput. Math. Appl. 65, 380–394.

Fang, F., Pain, C.C., Navon, I.M., Piggott, M.D., Gorman, G.J., Allison, P., Goddard, A.J.H., 2009. A POD reduced order unstructured mesh ocean modelling method for moderate Reynolds number flows ocean modelling. Ocean Models 28 (1–3), 127–136.

Fang, F., Pain, C.C., Navon, I.M., Piggott, M.D., Gorman, G.J., Allison, P., Goddard, A.J.H., 2009. Reduced order modelling of an adaptive mesh ocean model. Int. J. Numer. Methods Fluids 59 (8), 827–851.

Fang, F., Pain, C.C., Navon, I.M., Elsheikh, A.H., Du, J., Xiao, D., 2013. Non-linear Petrov-Galerkin methods for reduced order hyperbolic equations and discontinuous finite element methods. J. Comput. Phys. 234, 540–559.

Fukunaga, K., 1990. Introduction to Statistical Recognition, Second ed.. In: Computer Science and Scientific Computing Series Academic Press, Boston.

Galletti, B., Bruneau, C.H., Zannetti, L, Iollo, A., 2004. Low-order modelling of laminar flow regimes past a confined square cylinder. J. Fluid Mech. 503, 161–170.

Holmes, P., Lumley, J.L., Berkooz, G., Rowley, C.W., 2012. Turbulence, Coherent Structures, Dynamical Systems and Symmetry. Cambridge University Press, ISBN 9781107008250.

Hoteit, I., Kohl, A., 2006. Efficiency of reduced-order, time-dependent adjoint data assimilation approaches. J. Oceanogr. 62 (4), 539–550.

Iollo, A., Lanteri, S., Desideri, J.A., 2000. Stability properties of POD-Galerkin approximations for the compressible Navier-Stokes equations. Theor. Comput. Fluid Dyn. 13, 377–396.

Kirby, M., Sirovich, L., 1990. Application of the Karhunen-Loève procedure for the characterization of human faces. IEEE Trans. Pattern Anal. Mach. Intell. 12 (1), 103–108.

Lumley, J.L., 1967. The structure of inhomogeneous turbulent flows. Atmos. Turbul. Radio Wave Propag., 166–178.

Nguyen, N.C., Peraire, J., 2008. An efficient reduced-order modeling approach for non-linear parametrized partial differential equations. Int. J. Numer. Methods Eng. 76, 27–55.

Pain, C.C., Umpleby, A.P., de Oliveira, C.R.E., Goddard, A.J.H., 2001. Tetrahedral mesh optimisation and adaptivity for steady-state for transient finite element calcutions. Comput. Methods Appl. Mech. Eng. 190, 3771–3796.

Pain, C.C., Piggott, M.D., Goddard, A.J.H., Fang, F., Gorman, G.J., Marshal, D.P., Eaton, M.D., Power, P.W., de Oliveira, C.R.E., 2005. Three-dimensional unstructured mesh ocean modelling. Ocean Models 10 (1–2), 5–33.

Pope, S.B., 2000. Turbulent Flows. Cambridge University Press ISBN 0-521-59886-9.

Robert, C., Durbiano, S., Blayo, E., Verron, J., Blum, J., le Dimet, F.X., 2005. A reduced-order strategy for 4D-VAR data assimilation. J. Mar. Syst. 57 (1–2), 70–82.

Robert, C., Blayo, E., Verron, J., Blum, J., le Dimet, F.X., 2006. Reduced-order 4d-var: a preconditioner for the incremental 4d-var data assimilation method. Geophys. Res. Lett. 33 (L18609), 1–4.

Saunier, O., Bocquet, M., Mathieu, A., Isnard, O., 2009. Model reduction via principal component truncation for the optimal design of atmospheric monitoring networks. Atmos. Environ. 43, 4940–4950.

Sirovich, L., 1987. Turbulence and the dynamics of coherent structures, part ii: symmetries and transformations. Quart. Appl. Math. 45, 573–582.

Sportisse, B., Djouad, R., 2000. Reduction of chemical kinetics in air pollution modeling. J. Comput. Phys. 164, 354–376.

Sportisse, B., Djouad, R., 2007. Use of proper orthogonal decompositions for the reduction of atmospheric chemistry. J. Geophys. Res. 112 (D06303) http://dx.doi.org/10.1029/2006JD007808.

Stefanescu, R., Navon, I.M., 2013. POD/DEIM nonlinear model order reduction of an ADI implicit shallow water equations model. J. Comput. Phys. 237, 95–114.

Vermeulen, P.T.M., Heemink, A.W., 2006. Model-reduced variational data assimilation. Mon. Weather Rev. 134, 2888–2899.

Wang, Z., Akhtar, I., Borggaard, J., Iliescu, T., 2012. Proper orthogonal decomposition closure models for turbulent flows: a numerical comparison. Comput. Methods Appl. Mech. Eng. 237240, 1026.

Willcox, K., Peraire, J., 2002. Balanced model reduction via the proper orthogonal decomposition. AIAA J. 40 (11), 2323–2330.

Xiao, D., Fang, F., Du, J., Pain, C.C., Navon, I.M., Buchan, A.G., Elsheikh, A.H., Hu, G., 2013. Non-linear Petrov-Galerkin methods for reduced order modelling of the Navier-Stokes equations using a mixed finite element pair. Comput. Methods Appl. Mech. Eng. 255, 147–157.

Xiao, D., Fang, F., Buchan, A.G., Pain, C.C., Navon, I.M., Du, J., Hu, G., 2014. Non-linear model reduction for the Navier-Stokes equations using the residual DEIM method. J. Comput. Phys. 263, 1–18.